On the AGATA performances at low γ-ray energies

E Clément, J Ljungvall, R M Pérez-Vidal, J Dudouet, L Ménager

On the AGATA performances at low γ-ray energies

E. Clément [a] J. Ljungvall [b] R. M. Pérez-Vidal [c] J. Dudouet [d]
L. Ménager [a]

[a] *Grand Accélérateur National d'Ions Lourds (GANIL), CEA/DRF-CNRS/IN2P3, F-14076 Caen Cedex 05, France*

[b] *Laboratoire de Physique des 2 infinis Irène Joliot-Curie, CNRS / Université Paris-Saclay / Université de Paris 91405 Orsay cedex, France*

[c] *INFN Laboratori Nazionali di Legnaro, IT-35020 Legnaro, Italy*

[d] *Université Lyon, CNRS/IN2P3, IP2I-Lyon, F-69622, Villeurbanne, France*

Abstract

The response function of the Advanced GAmma Tracking Array (AGATA) at low energy has been evaluated with γ-ray sources from 20 keV to 1.4 MeV. Particular interest was given to the treatment of γ-ray below 100 keV which interact predominantly by photo-electric effect in the first centimeter of the germanium crystal. The performances are evaluated and improvements to the data processing are proposed.

Key words: AGATA spectrometer, γ-ray tracking, Pulse Shape Analysis

1 Introduction

High-resolution γ-ray spectroscopy plays a major role in nuclear structure, nuclear astrophysics and nuclear reaction mechanism studies. Continuous progress in detector technology and data analysis lead to improved sensitivity giving access to more exotic nuclei and detailed nuclear spectroscopic information. In recent years, dedicated set-ups coupling large high-purity Ge arrays and ancillary detectors, such as magnetic spectrometers or separators, scintillators for high energy γ-ray detection or fast-timing measurements, and particle detectors, have been developed in large scale heavy-ions facilities. Thanks to these improvements, high resolution γ-ray spectroscopy of exotic nuclei was performed with unprecedented sensitivity from light to heavy nuclei and from the proton to the neutron drip-lines [1]. In the quest of the study of heavy elements, new reaction mechanisms are proposed using heavy ions collisions

Preprint submitted to Nucl. Inst. and Meth. in Phy. Res. AReceived: 14 September 2022

above the Coulomb barrier [2–4]. In order to perform their prompt γ-ray spectroscopy, high performance magnetic spectrometers are required to identified the produced isotopes. In spite of their high performances,the unique element identification is not possible due to the low energy of the produced recoil and it is proposed to use the atomic x-rays emitted at the target position, to identify the element number. In this particular framework, the performances of AGATA [5] and the response function of the Pulse Shape Analysis and Tracking algorithms for photons below 100 keV are investigated in the present manuscript.

2 Source measurements

The AGATA response function was measured from 24.0 keV to 1.4 MeV with a particular focus on γ-rays energies below 100 keV using radioactive sources of ^{113}Sn ($T_{1/2}$= 115 days), ^{141}Ce ($T_{1/2}$= 32.5 days), ^{152}Eu ($T_{1/2}$= 13.33 years) and ^{203}Hg ($T_{1/2}$= 46.59 days) placed at the center of the array (see table 1). Individual crystal counting rate was kept between 100 and 500 Hz. A 15 keV electronic threshold was reached in the measurement. The data processing follows the usual AGATA procedure and Pulse Shape Analysis is performed on an event-by-event basis using the Adaptive Grid Search and the ADL libraries [5]. The individual crystal event are merged in software using a coincidence windows of 500 ns based on the GTS timestamp distribution. The OFT tracking algorithm is used with standard parameters [6]. Below 100 keV, several difficulties impact on the treatment a such interactions for γ tracking arrays. Indeed, the γ-rays absorption will mainly process by a single interaction in a photoelectric event at the very front of the AGATA crystal [5] where electric fields are the less coaxial due to the crystal shape, and with very low signal amplitude suffering from electronic noise which can impact the quality of the Pulse Shape Analysis [7].

3 Results

A schematic figure of an AGATA crystal is shown in figure 1. More details can be found in [8]. The (X,Y) coordinates define the slices with index "1" of the 6 front segments facing the radioactive sources. The Z coordinate corresponds to the depth in the cristal, the last slice of segment being number "6".

The results of the measurements are shown in figure 2. The top figure is shown in logarithmic scale in energy to highlight from the low energy part to the high energies regime. The bottom figure is in linear scale and zoomed on

Table 1
X-rays measured in the present work

Source	Energy [keV]	Intensity
^{152}Eu	39.52	21.0 %
	40.118	37.7 %
	45.293	3.75 %
	45.414	7.26 %
	46.578	2.40 %
^{141}Ce	35.55	4.90 %
	36.026	8.85 %
	40.748	1.67 %
^{203}Hg	70.83	3.69 %
	72.873	6.19 %
	82.574	1.43 %
^{113}Sn	24.00 + 24.21	28.0% + 51.8%
	27.23 + 27.27 + 27.86	4.66% + 9% + 2.39%

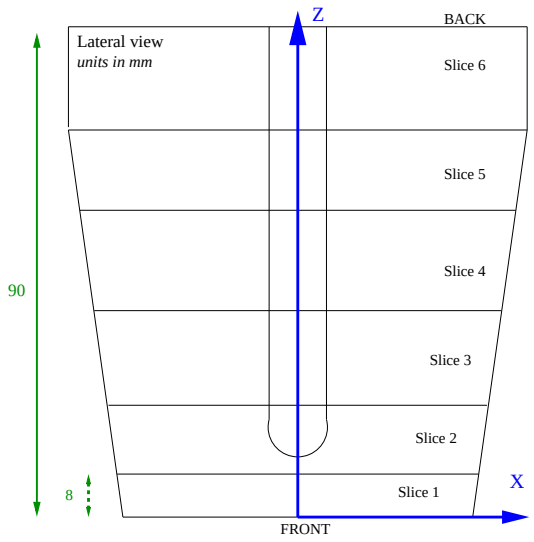

Fig. 1. (Color online) The schematic lateral view of an AGATA crystal. The figure shows the numbering of the slice from 1 (front, facing the source) to 6 (back). The first slice has a reduced size of 8 mm. More details in [8]

the x-ray region. The different experimental points show the relative efficiency obtained using different data processing, as described in the following section, and normalised to the γ-ray intensity measured in the core signal.

3.1 Segment procedure

The black points represent the normalized intensities measured in the electric segment, i.e. from individual hits before the tracking filter. Below 100 keV, the ratio is close to 1 since the interaction occurs with a single photoelectric process within a single electric segment. Beyond this turning point, the contribution of the Compton scattering between individual segment increases leading to a relative efficiency which decreases until $\simeq$ 1 MeV and saturates at $\simeq$ 0.20 indicating 20% of "single" interaction in a segment. Multiple interactions in a given segment are not separated in the present process.

3.2 Add-back procedure

The red squares shows the relative efficiency after an Add-back procedure of the neighbouring core output [9]. Below 200 keV, the incident photons is absorbed in the large volume of the HPGe crystal and the relative efficiency is close to 1. Beyond, Compton scattering between crystal occurs and an Add-back factor of 1.35 is reached at the 1.4 MeV ^{152}Eu line. One can noticed that the procedure induces a loss of intensity below 40 keV. One can speculate that a single interaction in a given crystal is added to noise from a neighbouring crystal. The loss is about 20% at 25 keV.

3.3 Tracking procedure

The green triangles shows the relative efficiency after OFT tracking. Above 80 keV, the OFT tracking performs as well as the core Add-back procedure with a better Peak-To-Total ratio in particular below 500 keV. Below 80 keV, in the x-rays area, a continues drop of the relative efficiency is observed. Such decrease is not reproduced in the OFT simulation using the interaction point from the GEANT4 simulation [10] and the same tracking parameters. For 40 keV γ-ray energy, GEANT4+OFT with the default packing of the simulated hits gives 60% of photopeak-efficiency with respect to the core output but measured at the level of 40%. This is attributed to Pulse Shape Analysis default in this energy regime. The AGATA processing allows a smearing of the hits positions determined by the Pulse Shape Analysis within the voxel. This has no effect on the efficiency as shown by the dark blue triangles.

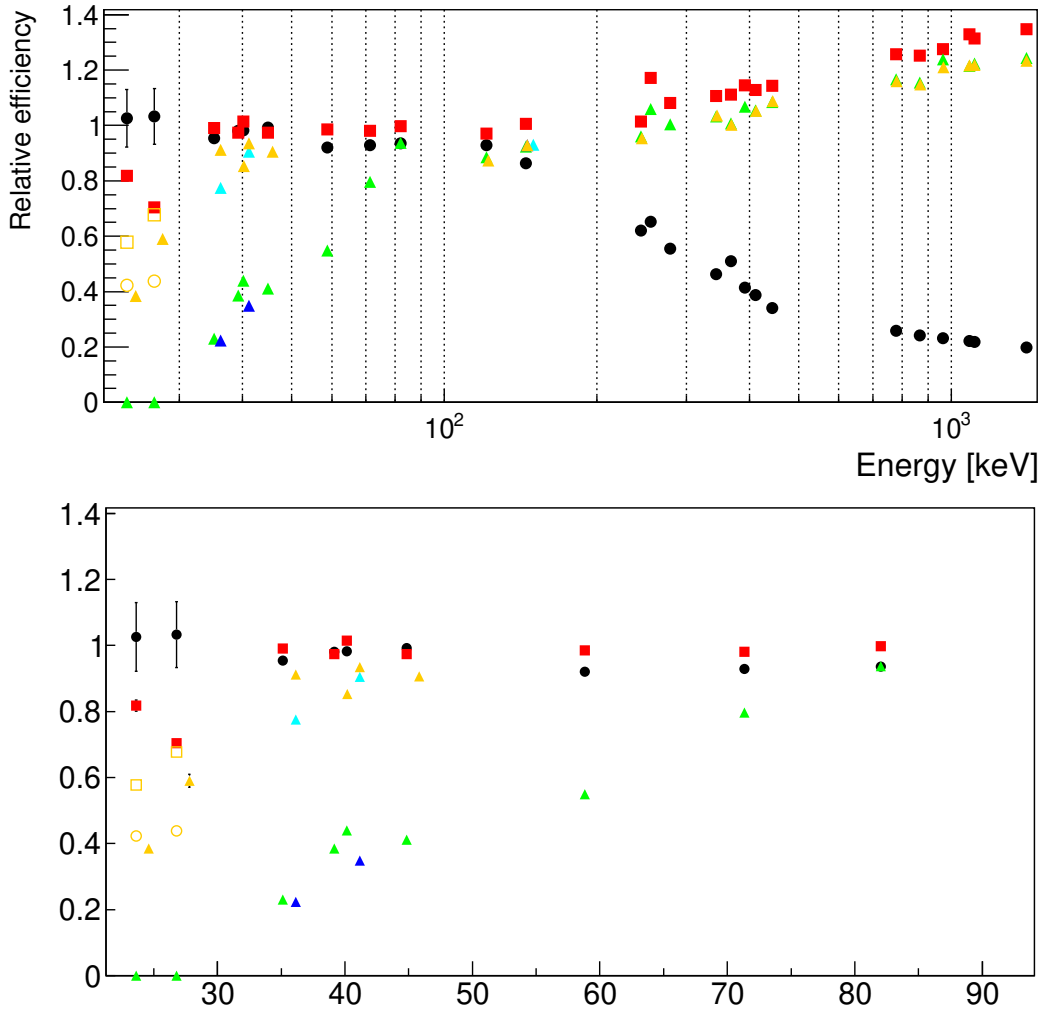

Fig. 2. (Color online) Relative efficiencies measurement as a function of the γ-ray energy (see text). Black : Segment energy. Red : Core Add-back. Green : Tracked. Dark blue : Tracked with smearing. Cyan triangle : 1mm correction. Orange triangle : 500 μm correction. Orange open squares : 100μm correction. Orange open circle 10μm correction.

3.4 Analysis of the non-tracked events

In this section, the photopeaks events rejected by the tracking algorithm are identified and analyzed. In the figure 3, the experimental hits distribution, computed by the Pulse Shape Analysis, as a function of the depth in the crystal (Z), gated on the ^{141}Ce x-rays is shown. The experimental distribution shows a flat pattern, randomly distributed between the entrance of the crystal and the end of the first slice at 10 mm. A distribution appears also at the back of the crystal (from 70 mm) and is attributed to either high energy photons entering by the crystal face and back-scattering in the cryostat, front-end electronic and LN2 dewar; or low energy photons from the room background entering

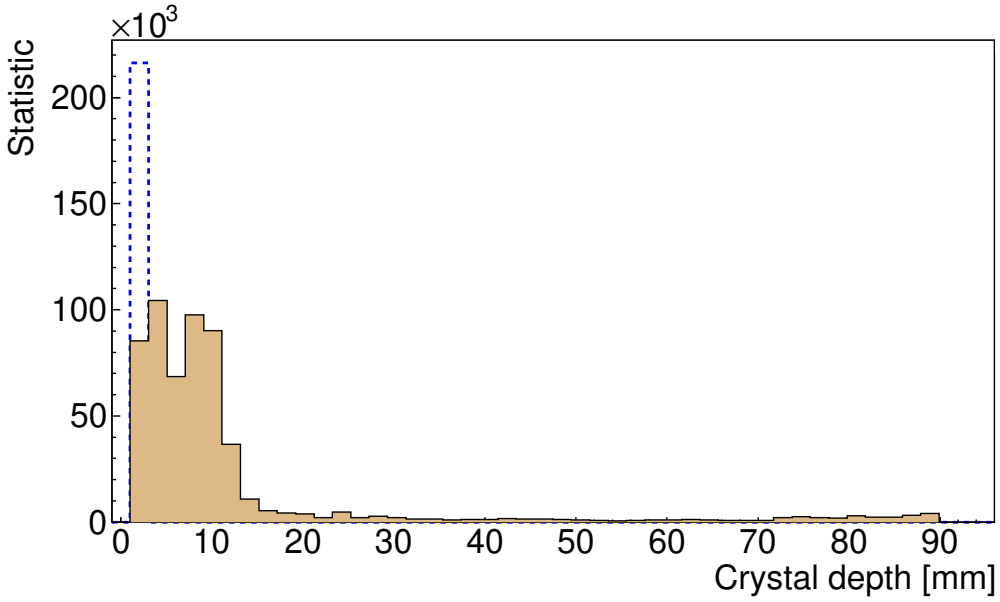

Fig. 3. (Color online) Experimental hits distribution as a function of the depth in the crystal gated on the ^{141}Ce x-rays. In blue, hits accepted by the tracking algorithms. In the filled histogram, rejected hits by the algorithm.

by the back of the crystal. The measured flat distribution below 15 mm is non physical since such low energy γ-ray must be absorbed within the first mm. The filled distribution shows the rejected hits by the tracking algorithm. The blue histogram shows the tracked events, which means hits accepted by the OFT algorithm and located by the Pulse Shape Analysis in the first millimiter of the crystal. OFT is identifying these events as a single photo-electric event which could only occur within the first two millimiters. One can also notice that the low energy events placed at the back of the crystal are well rejected by the OFT tracking algorithm.

The figure 4 shows the corresponding GEANT4 simulation for the ^{141}Ce x-rays energy. The distribution is well centered on the first millimiter as expected and disagrees with the experimental distribution. This disagreement leads to a high rejection of the hits by the OFT algorithm.

The spatial distribution of accepted and rejected hits is further analyzed. The (X,Y) distributions in the first front slice (segment 1 in figure 1) of the corresponding events are shown in figure 5. Figure a (b) shows the accepted (rejected) hits by the OFT tracking. The Z scale is identical. The distribution of the rejected hits is rather uniform as the accepted hits distributions shows a deficit in the middle of the crystal surface. The hit distributions are converted into radius coordinate (from central contact to crystal side) as a function of Z in figure 6. The radius is determined for the accepted (rejected) in blue (filled) interactions showing a specific pattern highlighting the large radius.

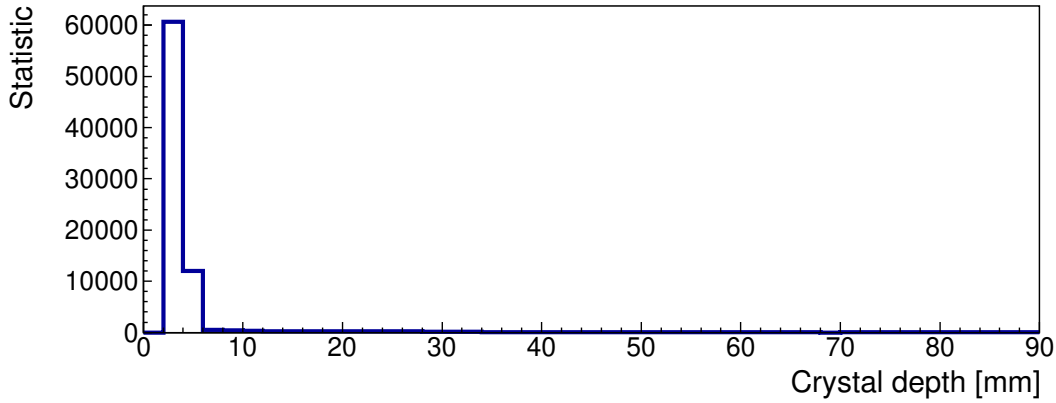

Fig. 4. (Color online) Simulated hits distribution as a function of the depth in the crystal gated on the ^{141}Ce x-rays.

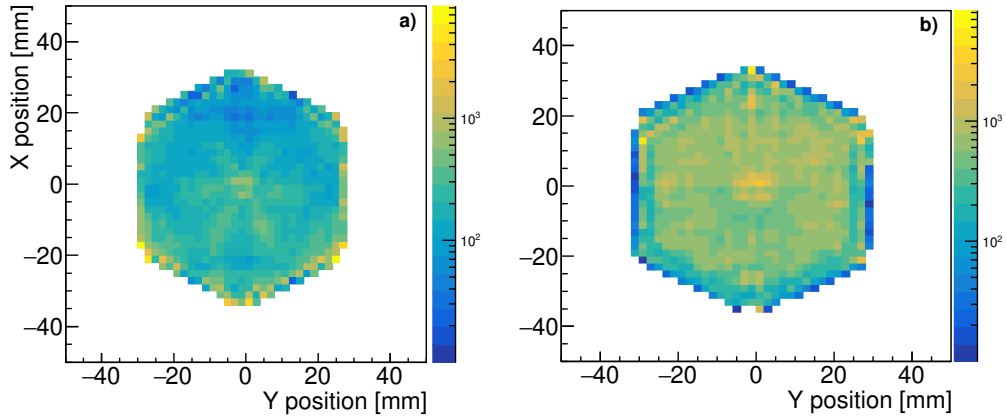

Fig. 5. (Color online) Two dimensional hits distribution for the front slice gated on the ^{141}Ce x-rays. (a) Accepted hits. (b) Rejected hits.

This significant pattern reflects the specifities of the low energy signals. We refer in the following to two other studies which have investigated the low energy signal in AGATA. Experimentaly, the low energy response function of highly segmented AGATA-type crystal was scanned at the IPHC scanning table [7]. The analysis of the 122 keV transition from ^{152}Eu reveals specific features. First it is demonstrated that, by opposition to energies greater than 200 keV, the database used presents overall large inconsistencies with the collected data. Also, already at 122 keV, the core and segment contacts have $\sim$5 keV and $\sim$2 keV noise on their maximum amplitude [7]. Much larger values can be extrapolated below 50 keV inducing, first, a large biais on the χ^2 method for the Pulse Shape Analysis and, secondly, impacting the time resolution and time alignment with respect to the reference database. Another very interesting observation is made in the scanned data. For such low energy signal, the transient signals amplitudes are small with respect to the net charge signal. At 122 keV, the transient signals are generally $\sim$ 15-10% except for the segment border where the segment signal is collected, it means at large radius, where they may rise up to $\sim$ 30% [7]. This larger amplitude lead to

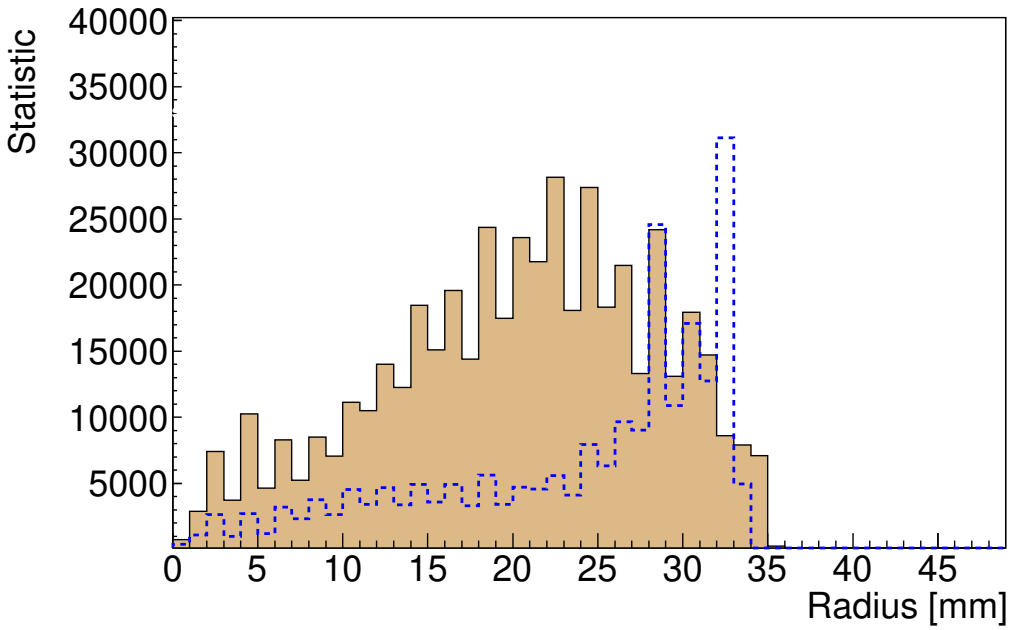

Fig. 6. (Color online) Distance to the central contact in the front slice gated on the on the ^{141}Ce x-rays for the front slice. In blue, hits accepted by the tracking algorithms. In the filled histogram, rejected hits by the algorithm.

higher signal-to-noise and better time resolution since it occurs closer to the signal collection. Therefore one can speculate that the Pulse Shape Analysis performs better leading to a better estimation of the Z coordinate and finally a higher acceptation rate by the OFT tracking as observed in figure 6.

Complementary to the general trend toward the side of the crystal, "hot spots" can identified in the corner of the crystal (beyond 32-33 mm) in figure 6. They were invetsigated by mean of simulation this time and these "hot spots" are most likely related to an incorrect determination of the start time for these events further enhanced by the low amplitude and noisy signal induced by the low energy γ-rays [11].

As a result, we support that the low efficiency observed at low energies in AGATA is due to a random estimation of the Z position by the PSA and not from the tracking algorithm.

The random character of the PSA results and its impact on the tracking is evaluated using the ADL bases directly. The grid positions in the first ring of the ADL basis for A002 are randomly extracted and processed in OFT for a 36 keV γ-ray. In the following, method 1 refers to the choice of random (X,Y,Z) positions and method 2 refers to a random distribution of Z into a (X,Y) column which mimic an accurate radius determination. The result of the corresponding Z distributions are shown in figure 8. The distribution is in agreement with the distribution of rejected event shown in figure 3.

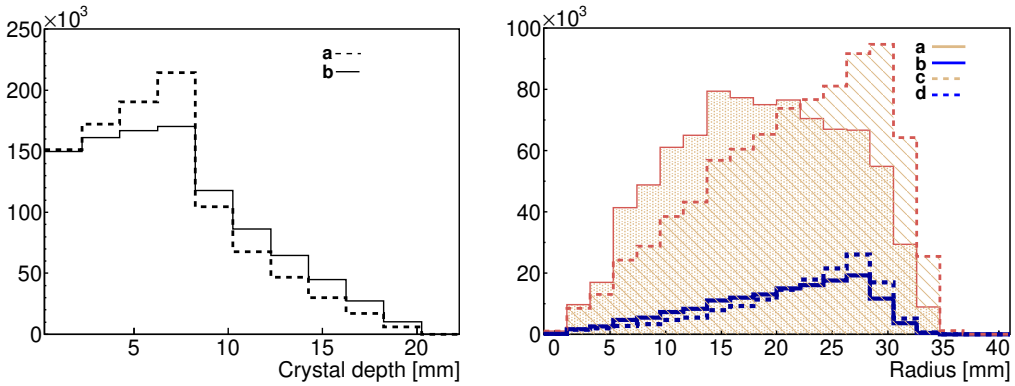

Fig. 7. (Color online) Left : Z distribution for random points in the first ring of an asymetric A-Capsule ADL bases. a, is for equal weights for each points (method 1) and b, is for equal weight for all (x,y) pairs (method 2). Right: Radial distribution for accepted (b,d) and rejected (a,c) events for random choices method 1 (a,b) and 2 (c,d)

The radial distribution is computed for accepted and rejected event using both method for the initial position. The distributions are shown in the figure. The agreement with figure 6 is reasonable with same trends. Similarly to the measurement, the accepted hits are more centered around large radius at 30 mm as the rejected hit distribution is centered at mid-radius and flat. The comparison between method 1 and 2 for the rejected hits seems to show that all coordinates are randomly determined and the measured distributions reflect only the grid granularity of the ADL bases convokuated with the shape of the crystal.

4 Post- Pulse Shape Analysis corrections

Post- Pulse Shape Analysis corrections are proposed before running the tracking algorithm to improve the efficiency at low energy. Before tracking, crystal events with a segment multiplicity equal one, an energy below 100 keV and located below 10 mm are selected. An arbitrary depth position is forced. We scanned different values to optimize the OFT efficiency. In figure 2, the position is forced to 1 mm (cyan triangle) and 0.5 mm (orange triangle). The 1 mm position allows to recover more than 90% efficiency as low as 40 keV as the 0.5 mm position allows to recover until 30 keV without impact at all the higher energies. An efficiency of 60-70% can be reached for the ^{113}Sn x-ray by adjusting the depth to 100 μm (orange squares). However, an even more shorter depth (10 μm orange circle) leads to a significant reduction of the gain reached with the 100 μm position showing that below 30 keV more advanced solutions are needed.

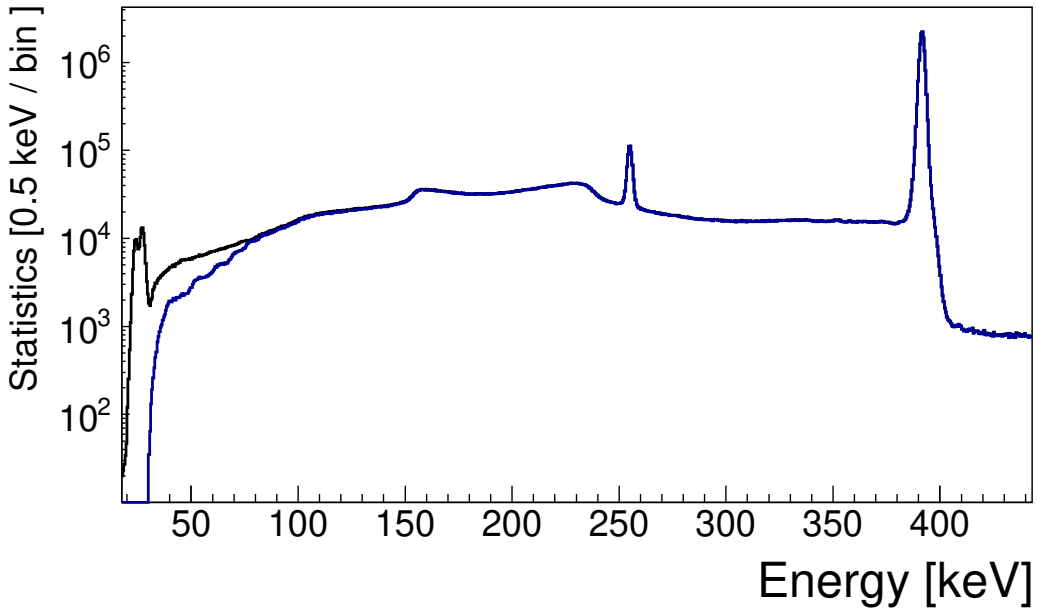

Fig. 8. (Color online) γ-ray spectrum of the β-decay of the ^{113}Sn source before (blue) and after (black) modified Pulse Shape Analysis for low energy event.

Figure 8 shows the γ-ray spectrum of the ^{113}Sn source placed at the center of AGATA with and without the corrections. The main γ-ray transitions at 255.1 keV (2.11(8)% intensity) and 391.7 keV (64.9(1) % intensity) are visible. The Kα (24 keV) and Kβ (27 keV) are visible only after applying the correction proposed in the present work, it means forcing the Z position to 100 μm, whereas they are suppressed by OFT using the standard PSA. As already mentionned, the low energy γ-rays measured at the back of the crystal coming from backing scattering are still rejected by the tracking algorithm after the correction, improving the peak-to-total ratio at low energy ($\leq$500 keV). This can be illustrated by an analysis of the peak-to-total ratio using the ^{152}Eu source. Considering all ^{152}Eu lines between 15 keV and 500 keV, the procedure leads to an improved peak-to-total ratio from 41.01(2)% to 44.14(8)% mainly coming from the improved efficiency of the x-ray detection. An integration from 65 keV to 500 keV, i.e excluding the x-ray contribution, leads to a similar peak-to-total ratio: 36.44(2)% and 35.14(6)% without and with correction, respectively, demonstrating that the procedure does not influence the quality of the spectrum in the energy range.

5 Conclusion

The low energy response function of AGATA below 100 keV down to 20 keV has been evaluated using a large set of low energy radioactive sources. It was demonstrated that the present Pulse Shape Analysis returns a random position

distribution in the first layer of the AGATA crystal for low energy (≤ 100 keV) interaction which highly impact the performances of the OFT tracking. New approaches which will reduce the noise of low amplitude trace signal and the time response will certainly improve the hit location at low energies. A simple patch is presented in this paper that allows to minimize the problem.

References

[1] A. Bracco, G. Duchene, Z. Podolyk, P. Reiter, Gamma spectroscopy with agata in its first phases: New insights in nuclear excitations along the nuclear chart, Progress in Particle and Nuclear Physics 121 (2021) 103887. doi:https://doi.org/10.1016/j.ppnp.2021.103887.
URL
https://www.sciencedirect.com/science/article/pii/S0146641021000417

[2] V. I. Zagrebaev, Y. T. Oganessian, M. G. Itkis, W. Greiner, Superheavy nuclei and quasi-atoms produced in collisions of transuranium ions, Phys. Rev. C 73 (2006) 031602. doi:10.1103/PhysRevC.73.031602.
URL https://link.aps.org/doi/10.1103/PhysRevC.73.031602

[3] A. Vogt, B. Birkenbach, P. Reiter, L. Corradi, T. Mijatović, D. Montanari, S. Szilner, D. Bazzacco, M. Bowry, A. Bracco, B. Bruyneel, F. C. L. Crespi, G. de Angelis, P. Désesquelles, J. Eberth, E. Farnea, E. Fioretto, A. Gadea, K. Geibel, A. Gengelbach, A. Giaz, A. Görgen, A. Gottardo, J. Grebosz, H. Hess, P. R. John, J. Jolie, D. S. Judson, A. Jungclaus, W. Korten, S. Leoni, S. Lunardi, R. Menegazzo, D. Mengoni, C. Michelagnoli, G. Montagnoli, D. Napoli, L. Pellegri, G. Pollarolo, A. Pullia, B. Quintana, F. Radeck, F. Recchia, D. Rosso, E. Şahin, M. D. Salsac, F. Scarlassara, P.-A. Söderström, A. M. Stefanini, T. Steinbach, O. Stezowski, B. Szpak, C. Theisen, C. Ur, J. J. Valiente-Dobón, V. Vandone, A. Wiens, Light and heavy transfer products in ^{136}Xe $+^{238}$ U multinucleon transfer reactions, Phys. Rev. C 92 (2015) 024619. doi:10.1103/PhysRevC.92.024619.
URL https://link.aps.org/doi/10.1103/PhysRevC.92.024619

[4] B. Birkenbach, A. Vogt, K. Geibel, F. Recchia, P. Reiter, J. J. Valiente-Dobón, D. Bazzacco, M. Bowry, A. Bracco, B. Bruyneel, L. Corradi, F. C. L. Crespi, G. de Angelis, P. Désesquelles, J. Eberth, E. Farnea, E. Fioretto, A. Gadea, A. Gengelbach, A. Giaz, A. Görgen, A. Gottardo, J. Grebosz, H. Hess, P. R. John, J. Jolie, D. S. Judson, A. Jungclaus, W. Korten, S. Lenzi, S. Leoni, S. Lunardi, R. Menegazzo, D. Mengoni, C. Michelagnoli, T. Mijatović, G. Montagnoli, D. Montanari, D. Napoli, L. Pellegri, G. Pollarolo, A. Pullia, B. Quintana, F. Radeck, D. Rosso, E. Şahin, M. D. Salsac, F. Scarlassara, P.-A. Söderström, A. M. Stefanini, T. Steinbach, O. Stezowski, S. Szilner, B. Szpak, C. Theisen, C. Ur, V. Vandone, A. Wiens, Spectroscopy of the neutron-rich actinide nucleus ^{240}U following multinucleon-transfer reactions, Phys. Rev. C 92 (2015) 044319. doi:10.1103/PhysRevC.92.044319.
URL https://link.aps.org/doi/10.1103/PhysRevC.92.044319

[5] S. Akkoyun, A. Algora, B. Alikhani, F. Ameil, G. de Angelis, L. Arnold, A. Astier, A. Ataac, Y. Aubert, C. Aufranc, A. Austin, S. Aydin, F. Azaiez, S. Badoer, D. Balabanski, D. Barrientos, G. Baulieu, R. Baumann, D. Bazzacco, F. Beck, T. Beck, P. Bednarczyk, M. Bellato, M. Bentley, G. Benzoni, R. Berthier, L. Berti, R. Beunard, G. L. Bianco, B. Birkenbach, P. Bizzeti, A. Bizzeti-Sona, F. L. Blanc, J. Blasco, N. Blasi, D. Bloor, C. Boiano, M. Borsato, D. Bortolato, A. Boston, H. Boston, P. Bourgault, P. Boutachkov, A. Bouty, A. Bracco, S. Brambilla, I. Brawn, A. Brondi, S. Broussard, B. Bruyneel, D. Bucurescu, I. Burrows, A. Burger, S. Cabaret, B. Cahan, E. Calore, F. Camera, A. Capsoni, F. Carrio, G. Casati, M. Castoldi, B. Cederwall, J.-L. Cercus, V. Chambert, M. E. Chambit, R. Chapman, L. Charles, J. Chavas, E. Clement, P. Cocconi, S. Coelli, P. Coleman-Smith, A. Colombo, S. Colosimo, C. Commeaux, D. Conventi, R. Cooper, A. Corsi, A. Cortesi, L. Costa, F. Crespi, J. Cresswell, D. Cullen, D. Curien, A. Czermak, D. Delbourg, R. Depalo, T. Descombes, P. Desesquelles, P. Detistov, C. Diarra, F. Didierjean, M. Dimmock, Q. Doan, C. Domingo-Pardo, M. Doncel, F. Dorangeville, N. Dosme, Y. Drouen, G. Duchene, B. Dulny, J. Eberth, P. Edelbruck, J. Egea, T. Engert, M. Erduran, S. Erturk, C. Fanin, S. Fantinel, E. Farnea, T. Faul, M. Filliger, F. Filmer, C. Finck, G. de France, A. Gadea, W. Gast, A. Geraci, J. Gerl, R. Gernhauser, A. Giannatiempo, A. Giaz, L. Gibelin, A. Givechev, N. Goel, V. Gonzalez, A. Gottardo, X. Grave, J. Grebosz, R. Griffiths, A. Grint, P. Gros, L. Guevara, M. Gulmini, A. Gorgen, H. Ha, T. Habermann, L. Harkness, H. Harroch, K. Hauschild, C. He, A. Hernandez-Prieto, B. Hervieu, H. Hess, T. Huyuk, E. Ince, R. Isocrate, G. Jaworski, A. Johnson, J. Jolie, P. Jones, B. Jonson, P. Joshi, D. Judson, A. Jungclaus, M. Kaci, N. Karkour, M. Karolak, A. Kaskas, M. Kebbiri, R. Kempley, A. Khaplanov, S. Klupp, M. Kogimtzis, I. Kojouharov, A. Korichi, W. Korten, T. Kroell, R. Krucken, N. Kurz, B. Ky, M. Labiche, X. Lafay, L. Lavergne, I. Lazarus, S. Leboutelier, F. Lefebvre, E. Legay, L. Legeard, F. Lelli, S. Lenzi, S. Leoni, A. Lermitage, D. Lersch, J. Leske, S. Letts, S. Lhenoret, R. Lieder, D. Linget, J. Ljungvall, A. Lopez-Martens, A. Lotode, S. Lunardi, A. Maj, J. van der Marel, Y. Mariette, N. Marginean, R. Marginean, G. Maron, A. Mather, W. Meczynski, V. Mendez, P. Medina, B. Melon, R. Menegazzo, D. Mengoni, E. Merchan, L. Mihailescu, C. Michelagnoli, J. Mierzejewski, L. Milechina, B. Million, K. Mitev, P. Molini, D. Montanari, S. Moon, F. Morbiducci, R. Moro, P. Morrall, O. Moller, A. Nannini, D. Napoli, L. Nelson, M. Nespolo, V. Ngo, M. Nicoletto, R. Nicolini, Y. L. Noa, P. Nolan, M. Norman, J. Nyberg, A. Obertelli, A. Olariu, R. Orlandi, D. Oxley, C. Ozben, M. Ozille, C. Oziol, E. Pachoud, M. Palacz, J. Palin, J. Pancin, C. Parisel, P. Pariset, G. Pascovici, R. Peghin, L. Pellegri, A. Perego, S. Perrier, M. Petcu, P. Petkov, C. Petrache, E. Pierre, N. Pietralla, S. Pietri, M. Pignanelli, I. Piqueras, Z. Podolyak, P. L. Pouhalec, J. Pouthas, D. Pugnere, V. Pucknell, A. Pullia, B. Quintana, R. Raine, G. Rainovski, L. Ramina, G. Rampazzo, G. L. Rana, M. Rebeschini, F. Recchia, N. Redon, M. Reese, P. Reiter, P. Regan, S. Riboldi, M. Richer, M. Rigato, S. Rigby, G. Ripamonti, A. Robinson, J. Robin, J. Roccaz, J.-A. Ropert, B. Rosse, C. R. Alvarez, D. Rosso, B. Rubio, D. Rudolph, F. Saillant, E. Sahin, F. Salomon, M.-D. Salsac, J. Salt, G. Salvato,

J. Sampson, E. Sanchis, C. Santos, H. Schaffner, M. Schlarb, D. Scraggs, D. Seddon, M. Senyigit, M.-H. Sigward, G. Simpson, J. Simpson, M. Slee, J. Smith, P. Sona, B. Sowicki, P. Spolaore, C. Stahl, T. Stanios, E. Stefanova, O. Stezowski, J. Strachan, G. Suliman, P.-A. Soderstrom, J. Tain, S. Tanguy, S. Tashenov, C. Theisen, J. Thornhill, F. Tomasi, N. Toniolo, R. Touzery, B. Travers, A. Triossi, M. Tripon, K. Tun-Lanoe, M. Turcato, C. Unsworth, C. Ur, J. Valiente-Dobón, V. Vandone, E. Vardaci, R. Venturelli, F. Veronese, C. Veyssiere, E. Viscione, R. Wadsworth, P. Walker, N. Warr, C. Weber, D. Weisshaar, D. Wells, O. Wieland, A. Wiens, G. Wittwer, H. Wollersheim, F. Zocca, N. Zamfir, M. Zieblinski, A. Zucchiatti, Agata advanced {GAmma} tracking array, Nuclear Instruments and Methods in Physics Research Section A: Accelerators, Spectrometers, Detectors and Associated Equipment 668 (2012) 26 – 58. doi:http://dx.doi.org/10.1016/j.nima.2011.11.081.

[6] A. Lopez-Martens, K. Hauschild, A. Korichi, J. Roccaz, J.-P. Thibaud, γ-ray tracking algorithms: a comparison, Nuclear Instruments and Methods in Physics Research Section A: Accelerators, Spectrometers, Detectors and Associated Equipment 533 (3) (2004) 454 – 466. doi:http://dx.doi.org/10.1016/j.nima.2004.06.154.

[7] B. D. Canditiis, G. Duchene, M. Sigward, F. Didierjean, M. Ginsz, D. Ralet, Full-volume characterization of an agata segmented hpge gamma-ray detector using a 152eu source, Eur. Phys. J. A 57 (2021) 223. doi:https://doi.org/10.1140/epja/s10050-021-00537-1.
URL
https://link.springer.com/article/10.1140/epja/s10050-021-00537-1

[8] A. Wiens, H. Hess, B. Birkenbach, B. Bruyneel, J. Eberth, D. Lersch, G. Pascovici, P. Reiter, H.-G. Thomas, The agata triple cluster detector, Nuclear Instruments and Methods in Physics Research Section A: Accelerators, Spectrometers, Detectors and Associated Equipment 618 (1) (2010) 223–233. doi:https://doi.org/10.1016/j.nima.2010.02.102.
URL
https://www.sciencedirect.com/science/article/pii/S0168900210003384

[9] G. Duchene, F. Beck, P. Twin, G. de France, D. Curien, L. Han, C. Beausang, M. Bentley, P. Nolan, J. Simpson, The clover: a new generation of composite ge detectors, Nuclear Instruments and Methods in Physics Research Section A: Accelerators, Spectrometers, Detectors and Associated Equipment 432 (1) (1999) 90–110. doi:https://doi.org/10.1016/S0168-9002(99)00277-6.
URL
https://www.sciencedirect.com/science/article/pii/S0168900299002776

[10] E. Farnea, F. Recchia, D. Bazzacco, T. Kroell, Z. Podolyak, B. Quintana, A. Gadea, Conceptual design and monte carlo simulations of the agata array, Nuclear Instruments and Methods in Physics Research Section A: Accelerators, Spectrometers, Detectors and Associated Equipment 621 (120133) (2010) 331 – 343. doi:http://dx.doi.org/10.1016/j.nima.2010.04.043.

[11] J. Ljungvall, Pulse-shape calculations and applications using the agatagefem

software package, Eur. Phys. J. A 57 (2021) 198. doi:10.1140/epja/s10050-021-00512-w.
URL https://doi.org/10.1140/epja/s10050-021-00512-w